Characterization and Classification of Zebrafish Brain Morphology Mutants

LAURA ANNE LOWERY,[1,2] GIANLUCA DE RIENZO,[1] JENNIFER H. GUTZMAN,[1] AND HAZEL SIVE[1,2]*

[1]Whitehead Institute for Biomedical Research, Nine Cambridge Center, Cambridge Massachusetts 02142

[2]Department of Biology, Massachusetts Institute of Technology, 77 Massachusetts Avenue, Cambridge, Massachusetts 02139

ABSTRACT

The mechanisms by which the vertebrate brain achieves its three-dimensional structure are clearly complex, requiring the functions of many genes. Using the zebrafish as a model, we have begun to define genes required for brain morphogenesis, including brain ventricle formation, by studying 16 mutants previously identified as having embryonic brain morphology defects. We report the phenotypic characterization of these mutants at several timepoints, using brain ventricle dye injection, imaging, and immunohistochemistry with neuronal markers. Most of these mutants display early phenotypes, affecting initial brain shaping, whereas others show later phenotypes, affecting brain ventricle expansion. In the early phenotype group, we further define four phenotypic classes and corresponding functions required for brain morphogenesis. Although we did not use known genotypes for this classification, basing it solely on phenotypes, many mutants with defects in functionally related genes clustered in a single class. In particular, Class 1 mutants show midline separation defects, corresponding to epithelial junction defects; Class 2 mutants show reduced brain ventricle size; Class 3 mutants show midbrain–hindbrain abnormalities, corresponding to basement membrane defects; and Class 4 mutants show absence of ventricle lumen inflation, corresponding to defective ion pumping. Later brain ventricle expansion requires the extracellular matrix, cardiovascular circulation, and transcription/splicing-dependent events. We suggest that these mutants define processes likely to be used during brain morphogenesis throughout the vertebrates. Anat Rec, 292:94–106, 2009.

Key words: zebrafish; brain morphology; mutants; brain structure; morphogenesis; neural tube; brain ventricle

Organ function is dependent not only on proper tissue specification but also on the three-dimensional organization of those tissues, directed by morphogenetic processes. In vertebrates, the embryonic brain originates from a simple columnar epithelium that forms a tube which will become the brain and spinal cord (Gray and Clemente, 1985). Brain morphogenesis occurs as the anterior neural tube undergoes a series of bends and constrictions to subdivide the brain into the future forebrain, midbrain, and hindbrain that allow it to pack into the skull. The first morphogenetic event is formation of a constriction at the midbrain–hindbrain boundary (MHB; Lowery and Sive, 2005). Another key event in brain morphogenesis is the opening of the brain ven-

Grant sponsor: NIH; Grant number: MH70926; Grant sponsor: NIH NRSA pre-doctoral fellowship, Abraham J. Siegel Fellowship, MIT/CSBi/Merck postdoctoral fellowship.

*Correspondence to: Prof. Hazel Sive, Nine Cambridge Center, Cambridge, MA 02142. Fax: 617-258-5578.
E-mail: sive@wi.mit.edu

Received 27 May 2008; Accepted 15 July 2008

DOI 10.1002/ar.20768

Published online 2 December 2008 in Wiley InterScience (www.interscience.wiley.com).

tricles, cavities inside the brain which contain cerebrospinal fluid (Lowery and Sive, 2005). Correct brain structure is intimately connected to normal brain function, as abnormalities in brain structure during development are correlated with a wide range of neurodevelopmental disorders (Kurokawa et al., 2000; Gilmore et al., 2001; Hardan et al., 2001; Rehn and Rees, 2005; Nopoulos et al., 2007).

Brain morphogenesis requires the function of many genes, but few have been well characterized. The zebrafish is an ideal model system for analysis of brain morphogenesis, since embryos can be live imaged at single-cell resolution, and mutants can be identified. The early structure of the zebrafish brain is very similar to that of other vertebrates, including chicken, rat and human, further indicating that this is a useful model system (Tropepe and Sive, 2003; Lowery and Sive, 2004; Jo et al., 2005). In order to identify the genetic mechanisms that regulate brain morphogenesis, we have examined 16 zebrafish brain mutants previously suggested to have abnormal embryonic brain morphology, identified in two large-scale mutagenesis screens (Jiang et al., 1996; Schier et al., 1996). Together Schier et al. (1996) and Jiang et al. (1996) identified 33 mutants with various embryonic brain morphology defects, 23 of which were described as having specific defects in embryonic brain ventricle morphology, through limited analyses. Through the generous sharing of the zebrafish community, we established 16 of these lines in our lab. In this report, we describe the brain phenotypes of these 16 mutants in more detail, including three mutants, *nagie oko, snakehead*, and *whitesnake*, on which we have published (Lowery and Sive, 2005; Lowery et al., 2007). On the basis of these data, we classify these mutants and describe some of the processes required for normal brain morphogenesis.

MATERIALS AND METHODS

Fish Lines and Maintenance

Danio rerio fish were raised and bred according to standard methods (Westerfield, 1995). Embryos were kept at 28.5°C and staged as described previously (Kimmel et al., 1995). Times of development are expressed as hours of postfertilization (hpf). All procedures on live animals and embryos were approved by the Massachusetts Institute of Technology Committee on Animal Care.

Lines used were: *snk*^{to273a}, *atl*^{tc234b}, *ott*^{ta76b}, *wis*^{tr241}, *vip*^{tw212e} (Jiang et al., 1996), *nok*^{m227}, *has*^{m567}, *ome*^{m98} (Malicki et al., 1996), *zon*^{m163}, *ful*^{m133}, *lnf*^{m551}, *log*^{m673}, *esa*^{m725}, *sly*^{m86} (Schier et al., 1996), *gup*^{hi1113B}(Amsterdam et al., 2004), *nat*^{tl43c} (Trinh and Stainier, 2004), *mot*$^{mot\_m807}$ (Guo et al., 1999). As *mot* and *ott* are allelic, these two alleles were used interchangeably in our mutant analysis.

Brain Ventricle Imaging

Brain ventricle imaging was performed as described previously (Lowery and Sive, 2005). Briefly, embryos were anesthetized in 0.1 mg/mL Tricaine (Sigma) dissolved in embryo medium prior to hindbrain ventricle microinjection with 2–10 nl dextran conjugated to rhodamine (5% in 0.2 mol/L KCl, Sigma), and then embryos were imaged by light and fluorescence microscopy with a Leica dissecting microscope, using a KT Spot Digital Camera (RT KE Diagnostic Instruments). Images were superimposed in Photoshop 6 (Adobe).

Immunohistochemistry

Whole-mount immunostaining was carried out using mouse anti-acetylated alpha tubulin (Sigma, 1:1000), mouse anti-neurofilament RM044 (Zymed no. 13-0500, 1:50), mouse anti-zn8 (Developmental Studies Hybridoma Bank, 1:20), and rabbit anti-Mpp5 polyclonal antibody (Wei and Malicki, 2002) (1:500). Goat anti-mouse Alexa Fluor 488 and anti-rabbit Alexa Fluor 488 (Molecular Probes, 1:500) were used as secondary antibodies.

For labeling with acetylated tubulin and RM044 antibodies, dechorionated 36 hpf embryos were fixed in 2% tricloroacetic acid for 3 hr at room temperature, washed in PBS, permeabilized in 0.5% Triton X in PBS and blocked in 0.5% Triton X, 10% normal goat serum, 0.1% BSA in PBS for 3 hr, prior to incubation in antibody. Brains were flat mounted in glycerol and imaged with confocal microscopy.

For labeling with zn8 antibody, dechorionated 30 hpf embryos were fixed in 4% paraformaldehyde overnight at 4°C, then rinsed in phosphate buffer and permeabilized in 0.5% Triton X in phosphate buffer. Blocking was done for 4 hr at room temperature in 0.5% Triton X, 10% normal goat serum, 0.1% BSA in phosphate buffer. Brains were flat mounted in glycerol and imaged with confocal microscope.

For labeling with anti-Mpp5 antibody and phalloidin-Texas Red, embryos were fixed in 4% paraformaldehyde for 2 hr at room temperature, then rinsed in PBS and dechorionated. Blocking was done for 4 hr at room temperature in 0.5% Triton X, 4% normal goat serum, in phosphate buffer. Phalloidin conjugated to Texas Red (Sigma, 1:1000) was used to label actin filaments.

To block pigmentation, embryos were incubated in 0.2 mM 1-phenyl-2-thiourea in embryo media beginning at 22 hpf.

Live Confocal Imaging

Boron-dipyrromethene (BODIPY) ceramide (Fl C5, Molecular Probes) was dissolved in dimethyl sulfoxide (DMSO) to a stock concentration of 5 mmol/L. Embryos were soaked in 50 nmol/L BODIPY ceramide solution overnight in the dark. The embryos were then washed, dechorionated, and placed in wells in 1% agarose for confocal microscopy. Confocal imaging was performed using a Zeiss LSM510 (laser scanning microscope, LSM), using standard confocal imaging techniques (Cooper et al., 1999). Confocal images were analyzed using LSM software (Zeiss) and Photoshop 6.0 (Adobe).

In Situ Hybridization

RNA probes containing digoxigenin-11-UTP were synthesized from linearized plasmid DNA for *pax2.1* (Krauss et al., 1996), *krox20* (Oxtoby and Jowett, 1993), *zic1* (Grinblat et al., 1998), and *shh* (Krauss et al., 1993) as described (Harland, 1991). Standard methods for hybridization and for single color labeling were used as described elsewhere (Sagerstrom et al., 1996). After staining, embryos were fixed in 4% paraformaldehyde over-

night at 4°C and washed in PBS prior to mounting in glycerol and imaging with a Nikon compound microscope.

RESULTS AND DISCUSSION

Mutants Can Be Classified Based on Brain Morphology and Timing of Phenotype Onset

We previously suggested that early brain morphogenesis in zebrafish occurs in two phases (Lowery and Sive, 2005). The first phase, occurring between 17 and 24 hpf, includes the shaping of the brain epithelium, as the straight neural tube undergoes regionally specific bends and opens to form the brain ventricles (Lowery and Sive, 2005). During the second phase, which occurs between 24 and 36 hpf, along with the onset of heartbeat and circulation, both the amount of brain tissue and the volume of the brain ventricles increase substantially (Lowery and Sive, 2005; Mueller and Wullimann, 2005; Bayer and Altman, 2007).

In order to examine the phenotypes of brain morphology mutants, we first analyzed initial brain morphogenesis of each mutant between 17 and 36 hpf using brightfield microscopy (Table 1; data not shown). One criterion for calling each mutant a "brain morphology" mutant is that it makes a healthy neural tube with no visible necrosis through at least 20 hpf (not shown), implying that earlier stages of neural development, including neurulation, are normal. We observed that the abnormal brain phenotypes of 13 mutants are obvious by 20–21 hpf, indicating that initial brain shaping and opening are perturbed. The remaining three mutants (*vip*, *nat*, *wis*) appear to have wild-type brain morphology until 28 hpf, at which point brain morphology defects become apparent, indicating that these mutants are defective in later brain expansion (Table 1).

Brain morphogenesis occurs on neuroepithelium that has already acquired initial anteroposterior and dorsoventral pattern. We therefore asked whether any early brain phenotypes result from patterning defects. We extended analyses of patterning performed by Schier et al., 1996 and Jiang et al., 1996 using *in situ* hybridization for the anteroposterior markers *krox20* and *pax2a*, and the dorsoventral patterning markers *shh* and *zic1*. No abnormalities are obvious, although we cannot exclude subtle perturbations (data not shown).

All 13 early mutants appear to have brain ventricles of reduced size, as assayed by brightfield microscopy. For these mutants, we extended analyses at two timepoints by injecting a fluorescent dye into the brain cavity to highlight the brain ventricular space (Lowery and Sive, 2005). From observation of the brain morphology defects, we determined that the 13 early brain mutants can be divided into four phenotypic classes. We did not use known genotypes for this classification, but based it solely on the specific morphological phenotypes we observed. It was notable, however, that where affected genes are known, mutants with defects in related genes cluster together, showing similar phenotypes. The four classes are:

- Class 1—Midline separation defects.
- Class 2—Reduced ventricle size.
- Class 3—MHB abnormalities.
- Class 4—Absence of lumen inflation.

Initial Brain Shaping—Class 1—"Midline Separation" Defects (*nok, ome, has, zon, atl*)

In Class 1 mutants, dye injection into the ventricles highlights that distinct locations along the brain tube midline appear to remain shut. We have termed this a defect in "midline separation". After neurulation in wild-type zebrafish, the neural tube is closed but shows a distinct midline (Lowery and Sive, 2004). Subsequently, the tube opens at the midline, leaving the ventricular space centrally (that is filled with fluid) (Fig. 1A). But in the five mutants that comprise this class, *nok, ome, has, zon*, and *atl*, brain ventricle injections show that midline separation is perturbed, and the hindbrain, in particular, does not open uniformly (Fig. 1B,C,E–L). In several of these mutants, opening of the forebrain and midbrain is also perturbed. At 24 hpf, either the brain midline does not open at all (as in *nok*, Fig. 1B, and in forebrain and midbrain of *zon*, Fig. 1H), or there are localized regions where the hindbrain tube does not separate at the midline (arrows, Fig. 1C,G–I). These phenotypes persist through at least 36 hpf (Fig. 1E,F,J–L). Thus, the defect is not simply a lack of lumen inflation, but may indicate that the neuroepithelial cells are abnormal and remain touching in discrete locations throughout the tube. This is visible both by brightfield microscopy after ventricle injection and also at higher resolution using live confocal imaging after soaking the embryos in BODIPY-ceramide (Fig. 2B,E).

As will be discussed further below, it is not clear why midline separation is abnormal in these mutants. One possibility is that cells are abnormally adhesive across the midline. Apicobasal polarity is disrupted in some of these mutants (see below) and this may be required for a loss of adhesion and cell separation at the apical surface. A second, related, possibility is that with loss of apicobasal polarity, cell junctions form across the midline, preventing midline separation. A third possible reason for midline separation defects is that cell shape and/or ability to move is abnormal. In general, high-pressure injection into the brain ventricles of these mutants cannot completely separate the neural tube midline, which therefore seems stuck shut in places (data not shown), however, the specific reasons that the midline does not separate will require additional analyses.

Three of the mutants in this group (*nok, ome, has*) correspond to mutations in genes previously implicated in epithelial polarity and junction formation. The most severe midline separation mutant is *nagie oko* (*nok*), which has a mutation in the *mpp5* gene encoding a MAGUK protein localized to apical junction complexes (Wei and Malicki, 2002). This mutant has an almost straight brain tube with no or little midline opening at 24 hpf (Fig. 1B). When dye is injected into the midline where the hindbrain ventricle normally opens, the dye does not diffuse into other areas of the brain, suggesting that the brain tube is stuck shut (Fig. 1B). This defect persists through 36 hpf (Fig. 1E). We have previously observed in histological sections that *nok* mutants have a disorganized epithelium with no continuous midline, although there are small, intermittent regions with a midline present (Lowery and Sive, 2005). We suggest that these obstructions in the midline correspond to locations where the brain tube is stuck shut.

TABLE 1. New classifications of brain morphology mutants

Brain phenotype (Class)	Locus[allele]	Gene	Gene function	Brain phenotype onset[a] (hpf)	Neuronal abnormalities[b] fb[c]	hb[d]	co[e]	Reference
Initial shaping and inflation								
Midline separation defects	*nok*^{m227}	*mpp5*	Junctions/epithelium	20				(Schier et al., 1996; Wei and Malicki, 2002)
(Class 1)	*has*^{m567}	*prkci*	Junctions/epithelium	21				(Schier et al., 1996; Horne-Badovinac et al., 2001)
	ome^{m98}	*crb2*	Junctions/epithelium	20				(Schier et al., 1996; Omori and Malicki, 2006)
	zon^{m163}	ND	ND	20		hb		(Schier et al., 1996)
	atl^{tc234b}	ND	ND	21				(Jiang et al., 1996)
Reduced ventricle	*ott*^{ta76b}	*med12*	Transcription	20		hb	co	(Jiang et al., 1996; Wang et al., 2006)
size (Class 2)	*ful*^{m133}	ND	ND	20		hb	co	(Jiang et al., 1996; Schier et al., 1996)
	lnf^{m551}	ND	ND	20		hb	co	(Schier et al., 1996)
	log^{m673}	ND	ND	20		hb[f]	co	(Schier et al., 1996)
	esa^{m725}	ND	ND	20	fb[g]			(Schier et al., 1996)
MHB abnormalities (Class 3)	*sly*^{m86}	*lamc1*	Extracellular matrix	21	fb	hb	co	(Jiang et al., 1996; Schier et al., 1996; Parsons et al., 2002)
	gup^{hi1113B}	*lamb1*	Extracellular matrix	21		hb	co	(Jiang et al., 1996; Schier et al., 1996; Parsons et al., 2002)
Absence of lumen inflation (Class 4)	*snk*^{to273a}	*atp1a1*	Na+K+ ATPase	19				(Jiang et al., 1996; Schier et al., 1996; Lowery and Sive, 2005)
Later brain ventricle expansion								
Reduced ventricle height	*vip*^{tw212e}	ND	ND[h]	28	ND	ND	ND	(Jiang et al., 1996)
	nat^{tl43c}	*fn1*	Extracellular matrix	28	ND	ND	ND	(Jiang et al., 1996; Trinh and Stainier, 2004)
Abnormal morphology	*wis*^{tr241}	*sfpq*	Splicing/transcription	28		hb[i]	ND	(Schier et al., 1996; Lowery et al., 2007)

ND, not determined; MHB, midbrain–hindbrain boundary.
[a]Other embryonic phenotypes may be visible earlier.
[b]It is noted when obvious neuronal abnormalities are detected by whole mount immunohistochemistry. Cells left blank indicate no abnormalities are detected, although there may be subtle defects which are not apparent.
[c]Axon scaffolds in the forebrain are labeled with acetylated tubulin antibody at 36 hpf.
[d]Reticulospinal neurons in the hindbrain are labeled with RM044 antibody at 36 hpf.
[e]Commissural neurons in the hindbrain are labeled with zn8 antibody at 30 hpf.
[f]The reticulospinal neurons of *log* were usually similar to wild-type, as shown in Fig. 4Q, but there were occasional missing neurons at low frequency (10–20%), with phenotypes similar to the other mutants in this group.
[g]The phenotype of *esa* mutants was quite variable, ranging from severely disrupted axon scaffolds to wild-type-like scaffolds.
[h]As the only obvious mutant phenotype other than reduced ventricle height is lack of heartbeat, we speculate that the *vip* gene is important for some aspect of heart development and function.
[i]Many reticulospinal neurons of *wis* were absent, as shown in Lowery et al., 2007.

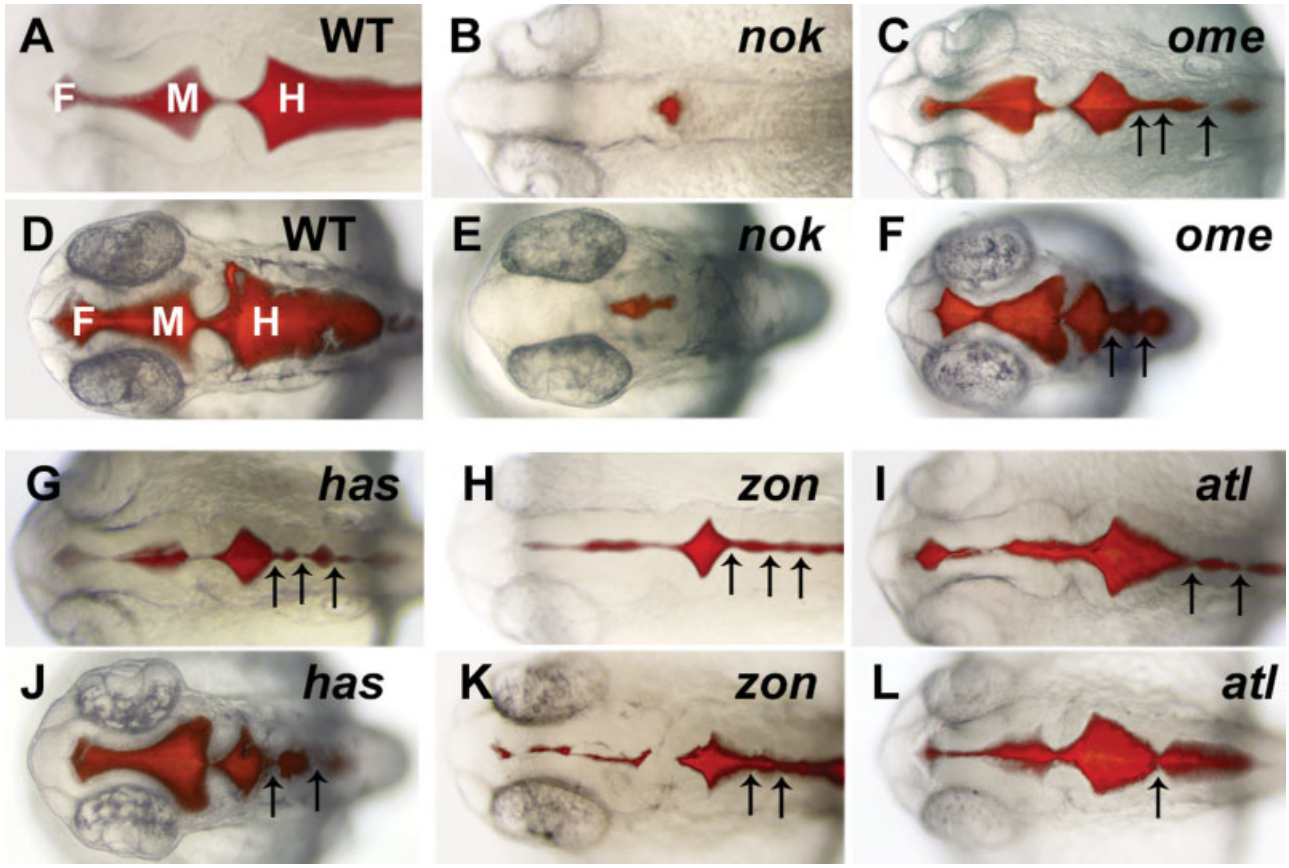

Fig. 1. Brain ventricle injections of *midline separation defects* mutants (Class 1, described in the text). Dorsal views of living, anesthetized embryos are shown, anterior to right, at 22 hpf (**A–C**,**G–I**) and 32–36 hpf (**D–F**,**J–L**) with brightfield microscopy. Ventricles are injected with rhodamine–dextran. Compared with WT (A,D), the left and right sides of the brain tube do not open uniformly in the midline separation mutants (B–L). In *nok* (B,E) dye injected into the hindbrain ventricle does not move. In the other mutants, (C,F) *ome*, (G,J) *has*, (H,K) *zon*, (I,L) *atl*, there are regions where the tube opens separated by places where the sides appear to be touching (arrows). The ventricles of WT are labeled for comparison. F: forebrain ventricle, M: midbrain ventricle, H: hindbrain ventricle.

Two mutants, *oko meduzy* (*ome*) and *heart and soul* (*has*) which have mutations in the *crb2a* and *prkci* genes, respectively (Horne-Badovinac et al., 2001; Omori and Malicki, 2006) display almost identical brain phenotypes. Both have relatively normal forebrain and midbrain shaping, but disrupted hindbrain opening, with several small openings instead of one large opening at 24 hpf (Fig. 1C,G), persisting through 36 hpf (Fig. 1F,J). Unlike the *nok* mutant (in which regions of the midline do not form), both *ome* and *has* appear to form a continuous midline throughout the neuroepithelium. Yet, the midline still does not separate in certain locations throughout the hindbrain.

The Mpp5, Crb2a, and Prkci proteins colocalize at the apical surface of neuroepithelia and control apical junction formation and epithelial apicobasal polarity (Horne-Badovinac et al., 2001; Hsu et al., 2006; Omori and Malicki, 2006), although the mechanisms underlying the brain phenotypes in these mutants have not yet been thoroughly explained. While the adherens junctions of the *nok* mutant are disrupted, as assayed by localization of adherens junction-associated actin foci (Lowery and Sive, 2005), the junctions in the brain epithelium of both *ome* and *has* mutants appear normal upon analysis of adherens junction-associated actin foci, even in the hindbrain regions (Fig. 3B,C), consistent with previous reports in other regions of the neuroepithelium (Horne-Badovinac et al., 2001; Omori and Malicki, 2006). However, localization of the apical junction protein, Mpp5 (mutated in *nok*), is partially disrupted in the *ome* mutant (Fig. 3E), but not in the *has* mutant (Fig. 3F). Whereas Mpp5 localizes solely to the apical junctions in wild-type neuroepithelia (Fig. 3D), in the *ome* mutant, Mpp5 is also mislocalized throughout the cells as assayed by immunohistochemistry (Fig. 3E). Thus, while the adherens junctions of these mutants appear normal according to actin localization, at least one junction component, Mpp5, is not properly localized in the *ome* mutant.

How do apical junction complex proteins regulate brain morphogenesis? In the case of the *nok* mutant, the neural tube midline is defective immediately after neurulation (Lowery and Sive, 2005), suggesting that Mpp5 may be required prior to neural tube closure, for normal epithelial integrity, apicobasal polarity, and formation of a midline corresponding to a plane of cell separation. In the case of *ome* and *has*, the neural tube does open in places, suggesting that the midline forms normally, and

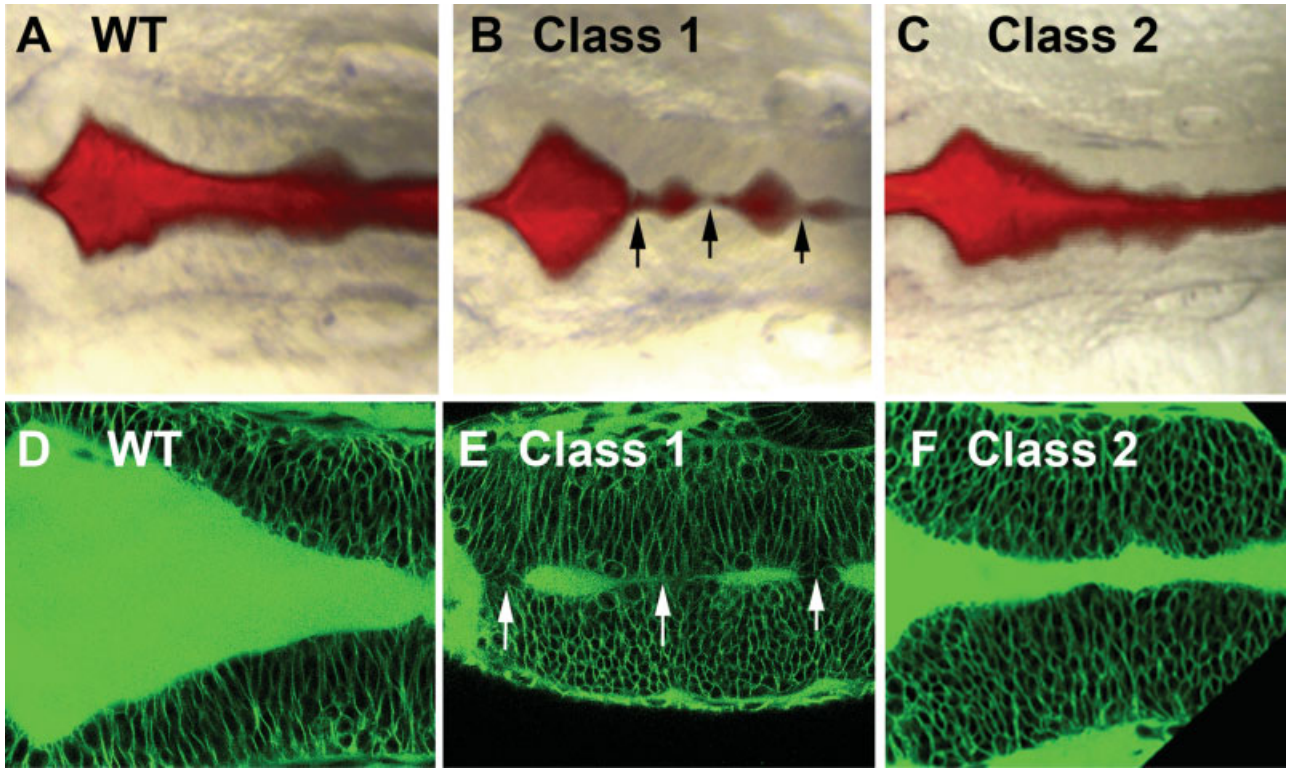

Fig. 2. Brain morphology comparison of Class 1 and Class 2. (**A–C**) Hindbrain dorsal views of living, anesthetized embryos are shown, anterior to right, at 22 hpf with brightfield microscopy, after dye injection. While Class 1 has locations along the brain tube where the left and right sides are opposed (B, *has* mutant), the sides of Class 2 brain tube separate normally (C, *lnf* mutant). (**D–F**) Hindbrain horizontal confocal sections after soaking embryos in BODIPY-ceramide to highlight cell outlines. Bright green identified hindbrain ventricle space. Neuroepithelial cells of Class 1 touch at the midline, or are perhaps fused (E, arrows, *zon* mutant), however fluid separates left and right sides of Class 2 (F, *lnf* mutant).

the adherens junction-associated actin localization appears normal. However, we observed that at least one apical component, Mpp5, is mislocalized in the *ome* mutant (Fig. 3E), and it is possible that other apicobasal polarity components are also disrupted. Thus, apicobasal polarity defects may lead to a neuroepithelium with compromised integrity and inability to separate at the midline. For example, during gut tube formation, *has* often shows multiple small lumens rather than one large one, because of a lack of apical clustering of adherens junctions (Horne-Badovinac et al., 2001). Further investigation will be required to determine the precise mechanisms that are disrupted in each mutant, and how these regulate midline separation. However, our analysis indicates that the apical junction components, Mpp5, Crb2a, and Prkci, may function together to promote neuroepithelial midline separation, and that Mpp5 apical localization requires function of Crb2a, but not Prkci.

Two additional mutants, *zonderzon* (*zon*) and *atlantis* (*atl*), corresponding to unknown mutations, also show variable midline separation defects. While the *zon* midline separation defect can be severe at 24 hpf (Fig. 1H) and persist through 36 hpf (Fig. 1K), the expressivity is variable. The *atl* mutant consistently shows a mild midline separation defect, with at least one point of contact at the midline within the hindbrain between 24 and 30 hpf (Fig. 1I,L, arrows). This mutant is the least severe of the group, and in some, the brain appears wild-type by 36 hpf. The *atl* mutant is also the only mutant described in this paper in which some homozygous mutants are viable. Further analysis of *zon* and *atl* and identification of their corresponding genes will be required to understand the underlying cause of the midline separation phenotype and if they are related to epithelial integrity.

One question we have considered is the relationship between early brain morphology and neuronal development and function. In particular, do any of these midline separation mutants also display neuronal abnormalities? We examined several axon tracts in the early embryo, looking at the early axon scaffolds in the forebrain and midbrain at 36 hpf, which can be visualized with an antibody to acetylated tubulin (Chitnis and Kuwada, 1990), at the reticulospinal neurons in the hindbrain at 36 hpf with an antibody to neurofilament M (Pleasure et al., 1989), and at commissural neurons in the hindbrain at 30 hpf with the zn8 antibody (Trevarrow et al., 1990). Within this mutant class, all neuronal tracts appear normal, although the *zon* mutant displays occasional defects of the reticulospinal neurons (data not shown). These data suggest that the midline separation defects in these mutants and formation of the early axon scaffold are under independent control.

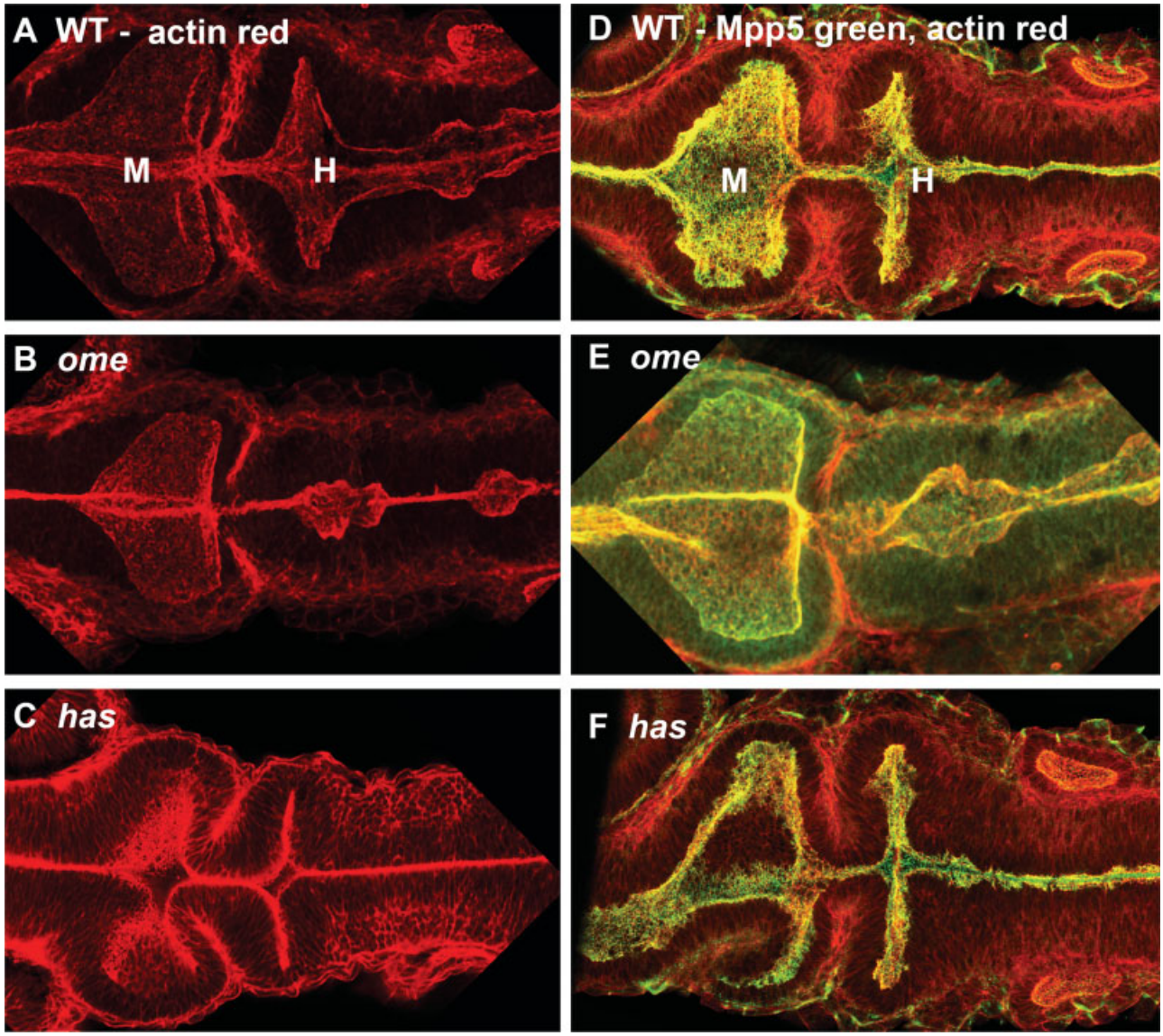

Fig. 3. Epithelial junction analysis of *ome* and *has* mutants. Confocal images of 24 hpf flat-mounted embryos in horizontal section through midbrain and hindbrain. (**A–C**) Phalloidin-Texas Red labels adherens junction-associated actin of wild type (A), *ome* mutant (B), *has* mutant (C). Actin is enriched at the apically localized adherens junctions, and actin localization is normal in the mutants. (**D–F**) Mpp5 antibody labeling (green) of wild type (D) *ome* mutant (E), and *has* mutant (F) with phalloidin-Texas Red as counterstain (red). Mpp5 is apically localized in wild-type. In *ome*, while some Mpp5 localizes normally to the junctions, it is also present throughout the entire neuroepithelium (E). Localization is normal in *has* (F). Part of the midbrain ventricular surface is not visible in the plane of section, but junctions are normal in those planes. M midbrain, H hindbrain.

Initial Brain Shaping—Class 2—Reduced Ventricle Size (*lnf, ful, ott, log, esa*)

The second class of early mutants, including *landfill* (*lnf*), *fullbrain* (*ful*), *otter* (*ott*), *logelei* (*log*), and *eraserhead* (*esa*), exhibit reduced brain ventricle size and occasional misshapen midbrain tissue at 24 and 36 hpf, but show no other significant phenotypic abnormalities of brain morphology (Fig. 4A–L). After dye injection into the ventricles, the phenotypes of these mutants may appear similar to those in Class 1 as described earlier, although several comparisons indicate that these classes are distinct. Ventricle injection at high pressure showed that the brain ventricles of all of these Class 2 mutants can open normally, and the midlines of these mutants appear to separate normally (Fig. 2C). Similarly, the adherens junction-associated actin foci localize normally in these mutants, and BODIPY-ceramide outlining of cells shows that the two sides of the brain tube do not touch as in Class 1 (data not shown, and Fig. 2F).

The brain phenotypes of *lnf*, *ful*, *ott*, and *log* are very similar, although at 24 hpf, *ott* ventricles are generally the most reduced in size, and *log* ventricles are the least reduced, relative to wild type (Fig. 4A–E). The *esa* phenotype, while

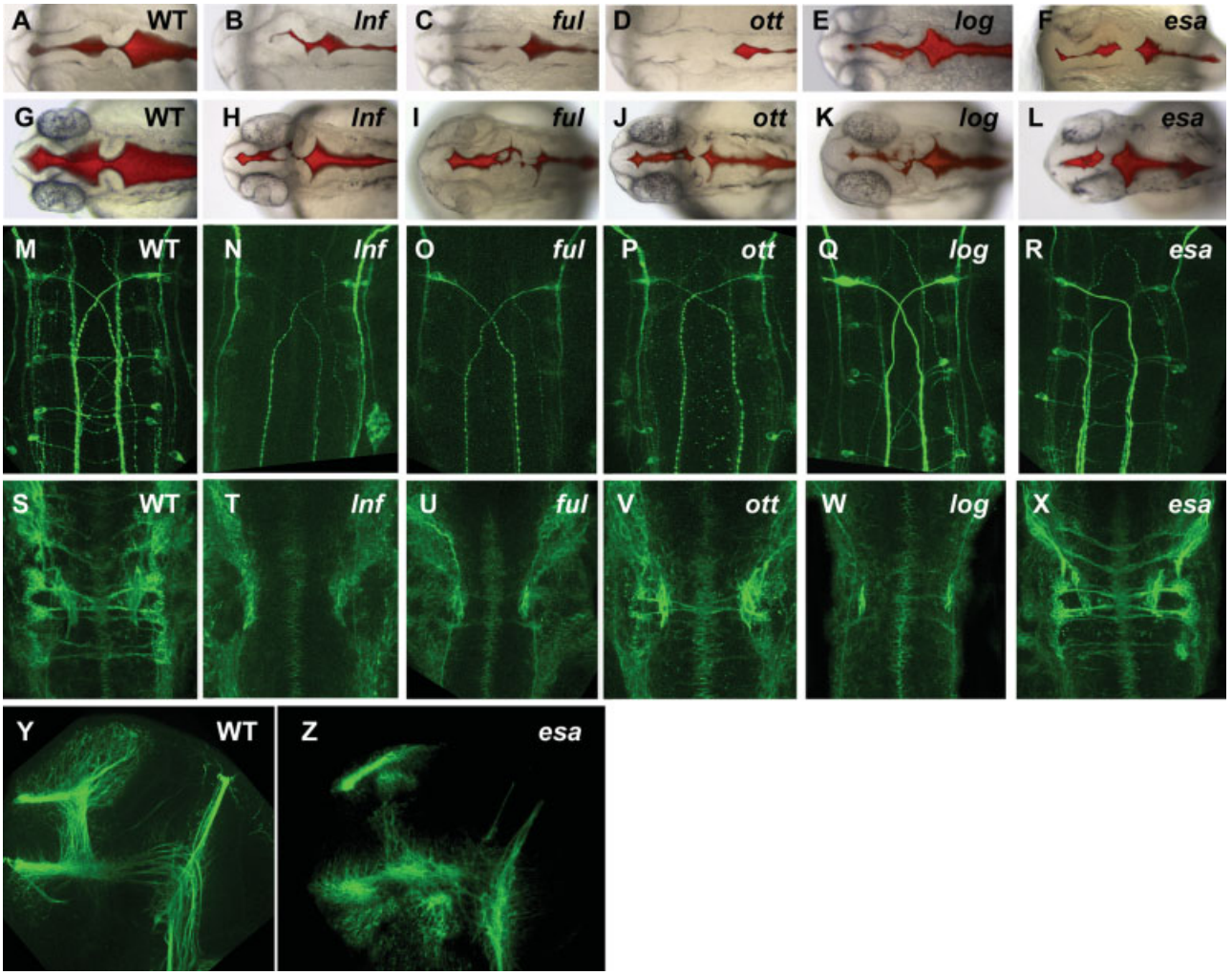

Fig. 4. Brain ventricle injections and antibody labelings for *reduced ventricle size* Class 2. Dorsal views of living, anesthetized embryos are shown, anterior to right, at 22 hpf (**A**–**F**) and 36 hpf (**G**–**L**) with bright-field microscopy. Ventricles are injected with rhodamine–dextran. The brain ventricles of *lnf* (B,H), *ful* (C,I), *ott* (D,J), *log* (E,K), and *esa* (F,L) are all similarly reduced compared to wild-type (A,G). (**M**–**R**) Dorsal views of 36 hpf hindbrain flatmounts, anterior is to the top, after labeling with the RMO44 Ab (reticulospinal neurons) shows reduced number of cell bodies and axons in *lnf* (N), *ful* (O), *ott* (P), and *log* (Q), compared to wild-type (M), although *esa* (R) appears similar to wild-type (M). (**S**–**X**) Dorsal views of 30 hpf hindbrain flatmounts, anterior is to the top, after labeling with the zn8 Ab (hindbrain commissural neurons) shows various levels of reduced commissures in *lnf* (T), *ful* (U), *ott* (V), and *log* (W), although *esa* (X) is indistinguishable from wild-type (S). (**Y**,**Z**) Lateral views of 36 hpf forebrain and midbrain flatmounts, anterior is to the left, dorsal is to the top, after labeling with acetylated tubulin Ab, which identifies the early axon scaffolds, shows that *esa* axonal pathfinding is severely disrupted, with the axons having a "feathered" appearance rather than fasciculating normally (Z), compared to wild-type (Y).

similar to the others in ventricle size reduction, is more variable (Fig. 4F,L) and is occasionally accompanied by additional brain and body phenotypes, which do not occur elsewhere in this class. These abnormalities include gastrulation defects (data not shown), which sometimes result in a twisting of the brain tissue (not shown).

Since the phenotypes of *ott*, *ful*, *lnf*, and *log* appear similar, complementation crosses were performed between them. Three individual crosses of *log* and *ott* heterozygote carriers resulted in 100% wild-type embryos (N = 154), demonstrating that *log* and *ott* do complement each other genetically. Crosses of all other mutant combinations also showed genetic complementation, indicating that each of these corresponds to a distinct locus. This is in contrast to a note added in the proof of (Schier et al., 1996) indicating that *logelei* does not complement *ott*.

We observed that the brain phenotypes of this mutant class resembles that of the mutants *motionless* (Guo et al., 1999) and *kohtalo* (Hong et al., 2005), which both have mutations in *med12*, a subunit of the mediator complex (Hong et al., 2005; Wang et al., 2006). A complementation cross between *mot* and *ott* resulted in 14 mutants (21%) and 54 wild-types (79%), suggesting that *ott* and *mot* are allelic, although the specific mutation in the *ott* mutant has not yet been reported. What role does the mediator complex play during development, and what could be responsible for the *ott* brain morphology phenotype? The mediator complex is a multiprotein complex that regulates transcription by acting as a

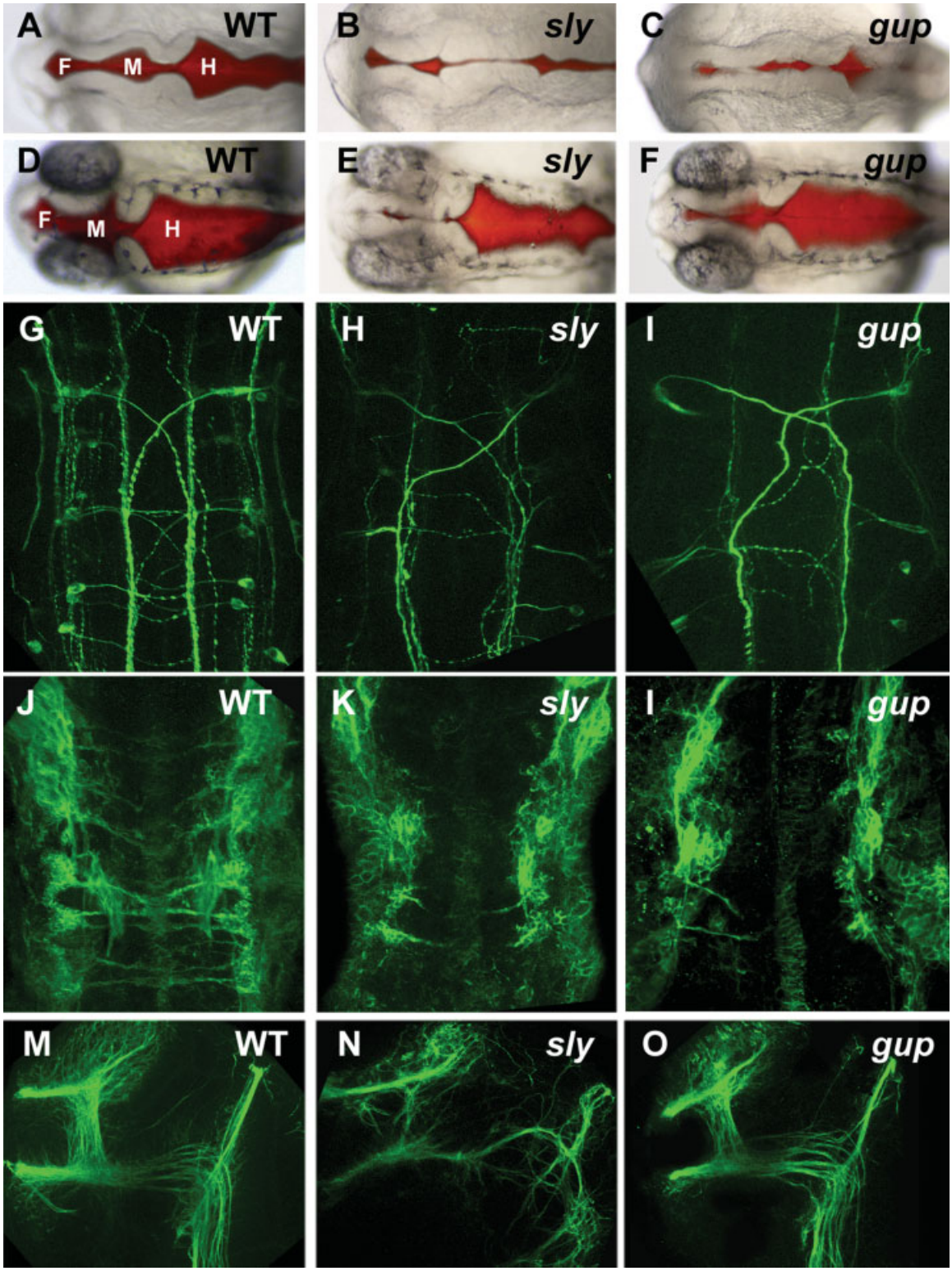

Fig. 5. Brain ventricle injections and neuronal antibody labelings for *MHB abnormalities* Class 3. Dorsal views of living, anesthetized embryos are shown, anterior to right, at 22 hpf (**A**–**C**) and 36 hpf (**D**–**F**) with brightfield microscopy. Ventricles are injected with rhodamine–dextran. At 22 hpf, both *sly* and *gup* (B,C) show an abnormal midbrain–hindbrain boundary. By 36 hpf, the *sly* and *gup* (E,F) boundary region has mostly recovered compared to WT (D), although the forebrain and midbrain ventricles are not as large as in WT. The ventricles of WT are labeled for comparison. F: forebrain ventricle, M: midbrain ventricle, H: hindbrain ventricle. (**G**–**I**) Dorsal views of 36 hpf hindbrain flatmounts, anterior is to the top, after labeling with the RMO44 Ab (reticulospinal neurons) shows disruption in axon pathfinding in both *sly* (H) and *gup* (I), compared to wild-type (G). (**J**–**L**) Dorsal views of 30 hpf hindbrain flatmounts, anterior is to the top, after labeling with the zn8 Ab (hindbrain commissural neurons) shows reduced commissures and disruption in axon pathfinding in both *sly* (H) and *gup* (I), compared to wild-type (G). (**M**–**O**) Lateral views of 36 hpf forebrain and midbrain flatmounts, anterior is to the left, dorsal is to the top, after labeling with acetylated tubulin Ab, which identifies the early axon scaffolds, shows that *sly* axonal pathfinding is disrupted (N), although *gup* (O) looks similar to wild-type (M).

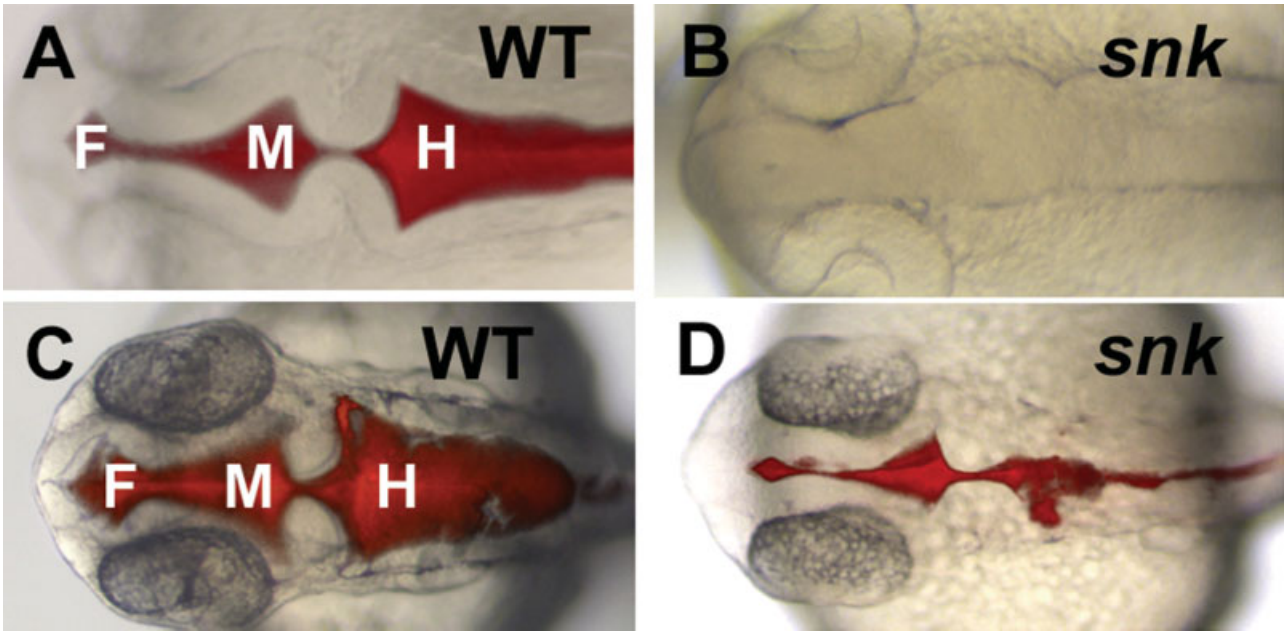

Fig. 6. Brightfield microscopy images of *absence of lumen inflation* mutant Class 4. Dorsal views of living, anesthetized embryos are shown, anterior to right. Wild-type embryos at 22 hpf (**A**) and 30 hpf (**C**). While the *snk* mutant at 22 hpf (**B**) has no visible ventricles and thus ventricles are not injected with dye, by 30 hpf (**D**), there are small ventricles in which dye can be injected, showing smaller but relatively normal shaping. F, forebrain ventricle; M, midbrain ventricle; H, hindbrain ventricle.

bridge between DNA-binding transcription factors and RNA polymerase II (Conaway et al., 2005). Several mediator subunits, including *med12*, possess gene-specific activity (Yoda et al., 2005; Rau et al., 2006; Loncle et al., 2007), and *med12* has been shown to interact with beta-catenin and transduce Wnt signaling (Kim et al., 2006). In the zebrafish *med12* mutant, the morphogenesis of many organ systems are affected as tissue extension, cell movements, and generation of tissue architecture are disrupted in various tissues (Hong et al., 2005). Interestingly, polymorphisms of the *med12* gene in humans are associated with an increased risk for schizophrenia (Philibert et al., 2007), a disorder which is correlated with abnormal brain structure and increased ventricle size (Antonova et al., 2004; Crespo-Facorro et al., 2007).

Zebrafish mutants deficient in *med12* display specific neuronal defects, though not all neurons are affected (Guo et al., 1999; Wang et al., 2006). We find that *lnf*, *ful*, and *ott* all show strong defects in the hindbrain axons, with reticulospinal and commissural neurons reduced or missing (Fig. 4N,P,T–V), although the early axon scaffolds in the forebrain and midbrain look normal (not shown). The *log* mutant has reduced commissural neurons (Fig. 4W) but all others appear normal (Fig. 4Q and not shown). The *esa* mutant phenotype is different than the others in that the reticulospinal and commissural neurons appear normal (Fig. 4R,X), but the axons in the forebrain and midbrain are severely (but variably) affected, having a "feathered" appearance (Fig. 4Z).

Initial Brain Shaping—Class 3—Midbrain–Hindbrain Boundary Abnormalities *(sly, gup)*

We defined Class 3 mutants as those which showed MHB abnormalities, in addition to reduced ventricles. Two mutants were placed into this class: *sleepy* (*sly*) and *grumpy* (*gup*). In these mutants, all brain ventricles are reduced in size compared to wild-type at 22 hpf (Fig. 5B,C). Additionally, the MHB appears abnormally shaped, in particular, the MHB fold that occurs by 22 hpf does not form normally (Fig. 5B,C), although by 36 hpf, MHB shape and hindbrain ventricle size are partially recovered (Fig. 5E,F). The *sly* and *gup* loci both encode components of the extracellular matrix (ECM) proteins, *laminin gamma1* and *laminin beta1*, respectively. These genes have previously been shown to play a number of roles during zebrafish developmental processes including notochord differentiation (Parsons et al., 2002), retina morphogenesis (Biehlmaier et al., 2007), blood vessel formation (Pollard et al., 2006), and retinotectal axon pathfinding (Karlstrom et al., 1996). As laminin in the basement membrane outlines the brain epithelium (data not shown), we hypothesize that loss of laminin in the basement membrane results in the inability to undergo normal brain epithelium shaping processes, particularly at the MHB (Gutzman et al., 2008).

Consistent with the previously reported role of laminin during axon guidance, we observed that the hindbrain reticulospinal neurons are disrupted in both mutants (Fig. 5H,I), as are the commissural neurons (Fig. 5K,L). Although the early axon scaffolds in the forebrain and midbrain are disorganized in the *sly* mutant (Fig. 5N), they are virtually indistinguishable from wild-type in the *gup* mutant, suggesting that *gup*/*lamb1* function is not essential for axonogenesis (Fig. 5O). It is possible that the mechanisms by which the axon defects arise in the *sly* and *gup* mutants are distinct from those regulating brain morphology.

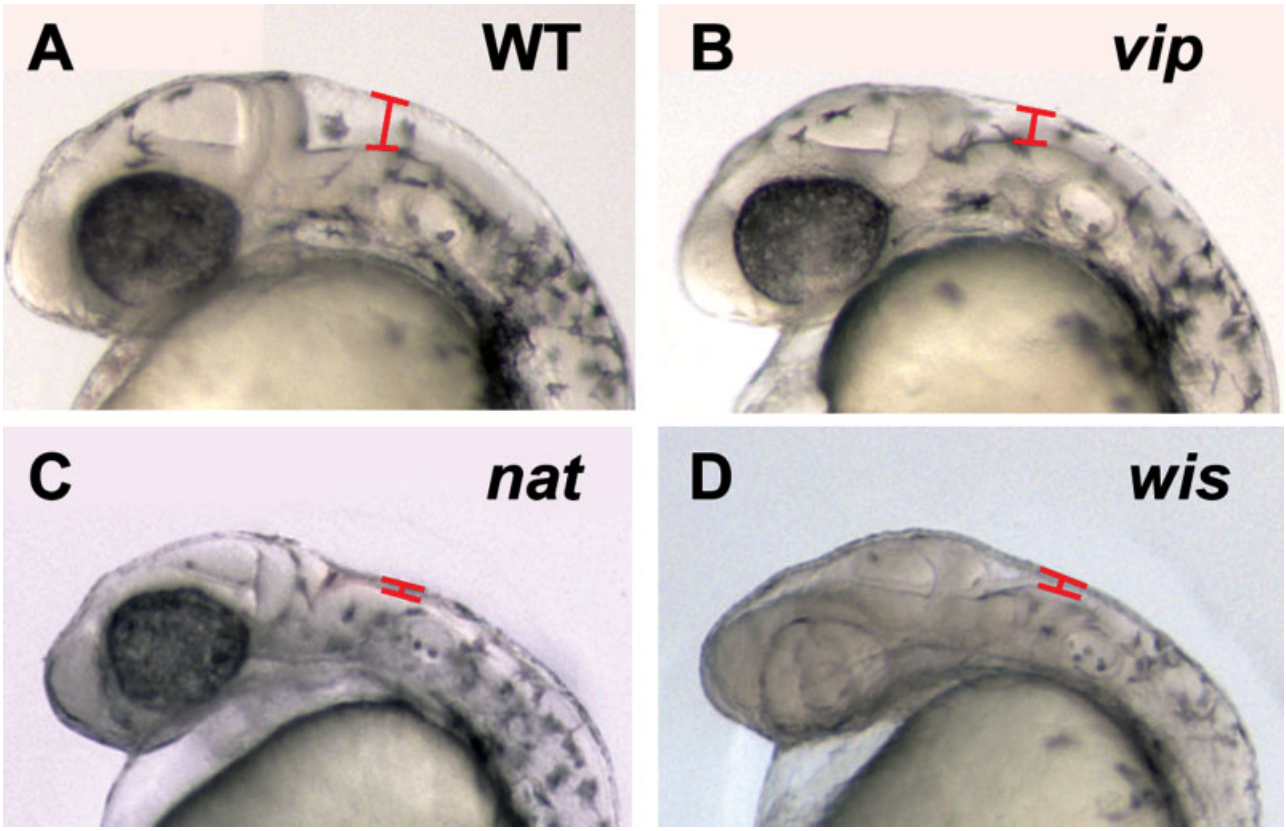

Fig. 7. Later brain ventricle expansion class. Lateral views of living, anesthetized embryos are shown, anterior to right, at 28 hpf, with brightfield microscopy. The *vip* mutant shows reduced hindbrain ventricle height (**B**, red bracket) compared to wild-type (**A**). The *nat* mutant shows more severe brain ventricle height reduction (**C**, red bracket). The *wis* mutant also shows significantly reduced hindbrain ventricle height (**D**, red bracket), in addition to reduced pigmentation and other brain morphology abnormalities not shown in this figure.

Initial Brain Shaping—Class 4—Absence of Lumen Inflation (*snk*)

One mutant was in a class by itself, based on its unique phenotype. The *snakehead* (*snk*) mutant lacks visible brain ventricles at 22 hpf by brightfield microscopy (Fig. 6B), and thus we did not perform ventricle dye injection at this stage. By 30 hpf, however, small ventricles are visible (Fig. 6D), and dye injection shows that *snk* brain morphology is similar to wild-type, with normal hingepoints indicative of normal brain morphogenesis. However, upon injection, all three ventricles are much smaller than normal. *snk* corresponds to a mutation in the *atp1a1* gene, encoding a Na^+K^+ ATPase alpha subunit (Lowery and Sive, 2005). This pump is likely required for embryonic CSF secretion by creating an ionic gradient across the membrane, which results in water flow into the luminal space (Lowery and Sive, 2005). It is likely that the absence of fluid inside the brain ventricles leads to the *snk* brain phenotype (Lowery and Sive, 2005). At the stages analyzed, we detected no obvious abnormalities in the neuronal populations examined (Table 1 and data not shown).

Later Brain Ventricle Expansion Mutants

In addition to the 13 early brain shape mutants described earlier, three brain morphology mutants, *viper* (*vip*), *natter* (*nat*), and *whitesnake* (*wis*) show only later defects in brain morphology. All three display normal brain ventricles at 22 hpf (data not shown), although by 28 hpf, it is apparent that the dorsoventral height of the hindbrain ventricle is reduced (Fig. 7B–D, bars). All three also lack heartbeat and circulation. It was previously shown that circulation is required for later brain ventricle expansion (Schier et al., 1996; Lowery and Sive, 2005), and thus, it is possible that the brain defects of these mutants are secondary to a lack of circulation. As the *vip* mutant shows no phenotypes other than reduced brain ventricle height and lack of heartbeat/circulation, and as the brain phenotype is similar to that of the *silent heart* mutant corresponding to a cardiac-specific troponin (Lowery and Sive, 2005), it is possible that the brain phenotype of this mutant is solely because of lack of circulation.

Conversely, the *nat* brain defect is more severe than the *vip* phenotype (compare Fig. 7B,C), and it is likely that the brain phenotype of this mutant is due to brain-specific effects as well as lack of circulation. The *nat* mutant corresponds to the fibronectin gene *fn1*, a component of the ECM, indicating that the ECM is essential for normal brain morphology, consistent with the requirement for laminin function (Class 3 mutants, Fig. 5) for initial brain shaping. However, the phenotypes of the laminin mutants *sly* and *gup* are different from *nat*, and appear earlier. This indicates that not all ECM com-

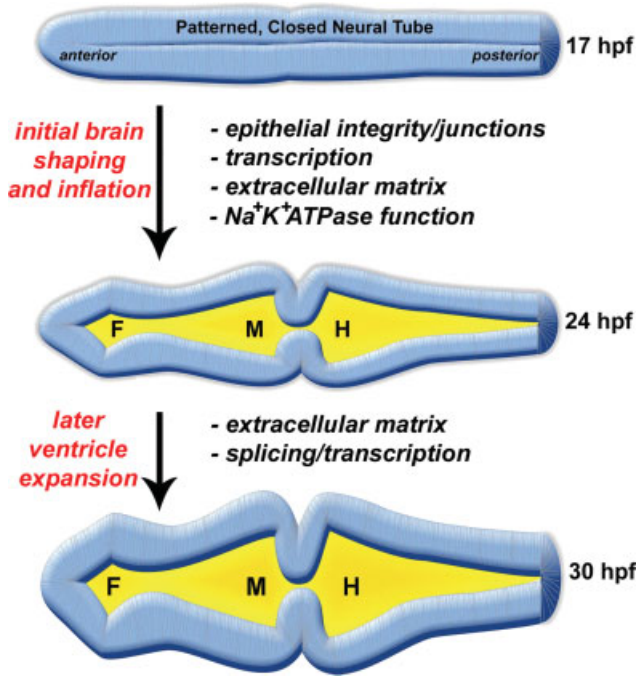

Fig. 8. Gene functions required for early brain morphogenesis. Processes involved in initial brain shaping and inflation include midline separation (requiring epithelial integrity/junctions), other mechanisms affecting brain morphology (requiring transcription, among other unknown factors), midbrain–hindbrain boundary formation (requiring extracellular matrix), and brain lumen inflation (requiring Na^+ K^+ ATPase activity). Later brain ventricle expansion requires the extracellular matrix in order to maintain normal ventricle height, as well as splicing/transcription, which contributes to normal brain morphology. F, forebrain ventricle; M, midbrain ventricle; H, hindbrain ventricle.

ponents are required at the same time or that the maternal contribution of fibronectin persists longer than that of laminin proteins.

The *wis* mutant has abnormalities in other aspects of embryonic brain morphology (not shown) in addition to the reduction in brain ventricle height (Fig. 7D), and further analysis of this mutant and its corresponding gene, *sfpq*, is described elsewhere (Lowery et al., 2007). This mutant has defects in neural development accompanied by increased cell death (Lowery et al., 2007), and these abnormalities may later result in abnormal brain morphology.

SUMMARY

Analysis of brain morphology mutants has allowed us to define several steps and corresponding gene functions required for brain morphogenesis (Fig. 8). Processes involved in initial brain shaping include midline separation, brain lumen inflation, MHB formation, and other mechanisms affecting brain morphology. Midline separation requires epithelial integrity and the apical junction components, *mpp5*, *prcki*, and *crb2*. The transcription regulator *med12*, which can affect early neuronal development (Guo et al., 1999; Wang et al., 2006), also has an effect on early brain morphology. The MHB formation requires the ECM protein laminin, specifically the *lamc1* and *lamb1* genes which encode the gamma and beta chains, respectively, components of the laminin heterotrimer. Brain lumen inflation requires the Na^+ K^+ ATPase, *atp1a1*. Later brain ventricle expansion requires the ECM protein fibronectin to maintain normal ventricle height, as well as the splicing/transcription factor *sfpq*, which contributes to normal brain morphology. There are certainly many more genes whose functions are required for brain morphogenesis, but were not identified in the mutant set we examined.

In conclusion, this detailed phenotypic characterization of 16 zebrafish brain mutants has enabled us to determine some of the various processes that are required for early brain morphogenesis. As embryonic brain ventricle morphology is conserved throughout the vertebrates, we suggest that these processes and their underlying mechanisms are also conserved.

ACKNOWLEDGMENTS

We thank members of the Sive Lab for helpful comments and Olivier Paugois for fish husbandry. We are very grateful to the Nusslein-Volhard lab for providing us with the *snk, atl, wis, vip*, and *ott* mutants, the Zebrafish International Resource Center for the *zon, ful, log, esa*, and *lnf* mutants, the Malicki lab for *nok, has*, and *ome*, and anti-Mpp5 antibody, the Zon lab for *sly*, the Hopkins lab for *gup*, and the Stainier lab for *nat*. The zn8 antibody developed by B. Trevarrow was obtained from the Developmental Studies Hybridoma Bank developed under the auspices of the NICHD and maintained by the University of Iowa, Department of Biogoical Sciences, Iowa City, IA 52242. This work was conducted utilizing the W.M. Keck Foundation Biological Imaging Facility at the Whitehead Institute.

LITERATURE CITED

Amsterdam A, Nissen RM, Sun Z, Swindell EC, Farrington S, Hopkins N. 2004. Identification of 315 genes essential for early zebrafish development. Proc Natl Acad Sci USA 101:12792–12797.

Antonova E, Sharma T, Morris R, Kumari V. 2004. The relationship between brain structure and neurocognition in schizophrenia: a selective review. Schizophr Res 70:117–145.

Bayer SA, Altman J. 2007. The human brain during the early first trimester. Boca Raton: CRC Press.

Biehlmaier O, Makhankov Y, Neuhauss SC. 2007. Impaired retinal differentiation and maintenance in zebrafish laminin mutants. Invest Ophthalmol Vis Sci 48:2887–2894.

Chitnis AB, Kuwada JY. 1990. Axonogenesis in the brain of zebrafish embryos. J Neurosci 10:1892–1905.

Conaway RC, Sato S, Tomomori-Sato C, Yao T, Conaway JW. 2005. The mammalian Mediator complex and its role in transcriptional regulation. Trends Biochem Sci 30:250–255.

Cooper MS, D'Amico LA, Henry CA. 1999. Confocal microscopic analysis of morphogenetic movements. Methods Cell Biol 59: 179–204.

Crespo-Facorro B, Barbadillo L, Pelayo-Teran JM, Rodriguez-Sanchez JM. 2007. Neuropsychological functioning and brain structure in schizophrenia. Int Rev Psychiatr 19:325–336.

Gilmore JH, van Tol JJ, Lewis Streicher H, Williamson K, Cohen SB, Greenwood RS, Charles HC, Kliewer MA, Whitt JK, Silva SG, Hertzberg BS, Chescheir NC. 2001. Outcome in children with fetal mild ventriculomegaly: a case series. Schizophr Res 48: 219–226.

Gray H, Clemente CD. 1985. Anatomy of the human body. 30th American ed. Philadelphia: Lea and Febiger.

Grinblat Y, Gamse J, Patel M, Sive H. 1998. Determination of the zebrafish forebrain: induction and patterning. Development 125: 4403–4416.

Guo S, Wilson SW, Cooke S, Chitnis AB, Driever W, Rosenthal A. 1999. Mutations in the zebrafish unmask shared regulatory pathways controlling the development of catecholaminergic neurons. Dev Biol 208:473–487.

Gutzman JH, Graeden E, Lowery LA, Holley H, Sive H. Formation of the midbrain-hindbrain boundary constriction requires laminin-dependent basal constriction. Mech Dev 125:974–983.

Hardan AY, Minshew NJ, Mallikarjuhn M, Keshavan MS. 2001. Brain volume in autism. J Child Neurol 16:421–424.

Harland RM. 1991. In situ hybridization: an improved whole-mount method for Xenopus embryos. Methods Cell Biol 36:685–695.

Hong SK, Haldin CE, Lawson ND, Weinstein BM, Dawid IB, Hukriede NA. 2005. The zebrafish kohtalo/trap230 gene is required for the development of the brain, neural crest, and pronephric kidney. Proc Natl Acad Sci USA 102:18473–18478.

Horne-Badovinac S, Lin D, Waldron S, Schwarz M, Mbamalu G, Pawson T, Jan Y, Stainier DY, Abdelilah-Seyfried S. 2001. Positional cloning of heart and soul reveals multiple roles for PKC lambda in zebrafish organogenesis. Curr Biol 11:1492–1502.

Hsu YC, Willoughby JJ, Christensen AK, Jensen AM. 2006. Mosaic Eyes is a novel component of the Crumbs complex and negatively regulates photoreceptor apical size. Development 133:4849–4859.

Jiang YJ, Brand M, Heisenberg CP, Beuchle D, Furutani-Seiki M, Kelsh RN, Warga RM, Granato M, Haffter P, Hammerschmidt M, Kane DA, Mullins MC, Odenthal J, van Eeden FJ, Nusslein-Volhard C. 1996. Mutations affecting neurogenesis and brain morphology in the zebrafish, Danio rerio. Development 123:205–216.

Jo H, Lowery LA, Tropepe V, Sive H. 2005. The zebrafish as a model for analyzing neural tube defects. In: Wyszynski DF, editor. Neural tube defects: from origin to treatment. New York: Oxford University Press. p 29–41.

Karlstrom RO, Trowe T, Klostermann S, Baier H, Brand M, Crawford AD, Grunewald B, Haffter P, Hoffmann H, Meyer SU, Muller BK, Richter S, van Eeden FJ, Nusslein-Volhard C, Bonhoeffer F. 1996. Zebrafish mutations affecting retinotectal axon pathfinding. Development 123:427–438.

Kim S, Xu X, Hecht A, Boyer TG. 2006. Mediator is a transducer of Wnt/beta-catenin signaling. J Biol Chem 281:14066–14075.

Kimmel CB, Ballard WW, Kimmel SR, Ullmann B, Schilling TF. 1995. Stages of embryonic development of the zebrafish. Dev Dyn 203:253–310.

Krauss S, Concordet JP, Ingham PW. 1993. A functionally conserved homolog of the Drosophila segment polarity gene hh is expressed in tissues with polarizing activity in zebrafish embryos. Cell 75:1431–1444.

Krauss S, Johansen T, Korzh V, Fjose A. 1991. Expression of the zebrafish paired box gene pax[zf-b] during early neurogenesis. Development 113:1193–1206.

Kurokawa K, Nakamura K, Sumiyoshi T, Hagino H, Yotsutsuji T, Yamashita I, Suzuki M, Matsui M, Kurachi M. 2000. Ventricular enlargement in schizophrenia spectrum patients with prodromal symptoms of obsessive-compulsive disorder. Psychiatry Res 99: 83–91.

Loncle N, Boube M, Joulia L, Boschiero C, Werner M, Cribbs DL, Bourbon HM. 2007. Distinct roles for Mediator Cdk8 module subunits in Drosophila development. EMBO J 26:1045–1054.

Lowery LA, Rubin J, Sive H. 2007. Whitesnake/sfpq is required for cell survival and neuronal development in the zebrafish. Dev Dyn 236:1347–1357.

Lowery LA, Sive H. 2004. Strategies of vertebrate neurulation and a re-evaluation of teleost neural tube formation. Mech Dev 121: 1189–1197.

Lowery LA, Sive H. 2005. Initial formation of zebrafish brain ventricles occurs independently of circulation and requires the nagie oko and snakehead/atp1a1a.1 gene products. Development 132: 2057–2067.

Malicki J, Neuhauss SC, Schier AF, Solnica-Krezel L, Stemple DL, Stainier DY, Abdelilah S, Zwartkruis F, Rangini Z, Driever W. 1996. Mutations affecting development of the zebrafish retina. Development 123:263–273.

Mueller T, Wullimann M. 2005. Atlas of Early Zebrafish Brain Development. Amsterdam: Elsevier.

Nopoulos P, Richman L, Andreasen NC, Murray JC, Schutte B. 2007. Abnormal brain structure in adults with Van der Woude syndrome. Clin Genet 71:511–517.

Omori Y, Malicki J. 2006. oko meduzy and related crumbs genes are determinants of apical cell features in the vertebrate embryo. Curr Biol 16:945–957.

Oxtoby E, Jowett T. 1993. Cloning of the zebrafish krox-20 gene (krx-20) and its expression during hindbrain development. Nucleic Acids Res 21:1087–1095.

Parsons MJ, Pollard SM, Saude L, Feldman B, Coutinho P, Hirst EM, Stemple DL. 2002. Zebrafish mutants identify an essential role for laminins in notochord formation. Development 129:3137–3146.

Philibert RA, Bohle P, Secrest D, Deaderick J, Sandhu H, Crowe R, Black DW. 2007. The association of the HOPA(12bp) polymorphism with schizophrenia in the NIMH genetics initiative for schizophrenia sample. Am J Med Genet B Neuropsychiatr Genet 144:743–747.

Pleasure SJ, Selzer ME, Lee VM. 1989. Lamprey neurofilaments combine in one subunit the features of each mammalian NF triplet protein but are highly phosphorylated only in large axons. J Neurosci 9:698–709.

Pollard SM, Parsons MJ, Kamei M, Kettleborough RN, Thomas KA, Pham VN, Bae MK, Scott A, Weinstein BM, Stemple DL. 2006. Essential and overlapping roles for laminin alpha chains in notochord and blood vessel formation. Dev Biol 289:64–76.

Rau MJ, Fischer S, Neumann CJ. 2006. Zebrafish Trap230/Med12 is required as a coactivator for Sox9-dependent neural crest, cartilage and ear development. Dev Biol 296:83–93.

Rehn AE, Rees SM. 2005. Investigating the neurodevelopmental hypothesis of schizophrenia. Clin Exp Pharmacol Physiol 32:687–696.

Sagerstrom CG, Grinbalt Y, Sive H. 1996. Anteroposterior patterning in the zebrafish, Danio rerio: an explant assay reveals inductive and suppressive cell interactions. Development 122:1873–1883.

Schier AF, Neuhauss SC, Harvey M, Malicki J, Solnica-Krezel L, Stainier DY, Zwartkruis F, Abdelilah S, Stemple DL, Rangini Z, Yang H, Driever W. 1996. Mutations affecting the development of the embryonic zebrafish brain. Development 123:165–178.

Trevarrow B, Marks DL, Kimmel CB. 1990. Organization of hindbrain segments in the zebrafish embryo. Neuron 4:669–679.

Trinh LA, Stainier DY. 2004. Fibronectin regulates epithelial organization during myocardial migration in zebrafish. Dev Cell 6:371–382.

Tropepe V, Sive HL. 2003. Can zebrafish be used as a model to study the neurodevelopmental causes of autism? Genes Brain Behav 2:268–281.

Wang X, Yang N, Uno E, Roeder RG, Guo S. 2006. A subunit of the mediator complex regulates vertebrate neuronal development. Proc Natl Acad Sci USA 103:17284–17289.

Wei X, Malicki J. 2002. nagie oko, encoding a MAGUK-family protein, is essential for cellular patterning of the retina. Nat Genet 31:150–157.

Westerfield M. 1995. The Zebrafish Book: a guide for the laboratory use of zebrafish, 4th ed. Eugene, Oregon: University of Oregon Press.

Yoda A, Kouike H, Okano H, Sawa H. 2005. Components of the transcriptional Mediator complex are required for asymmetric cell division in C. elegans. Development 132:1885–1893.